JOURNAL OF SPACECRAFT AND ROCKETS
Vol. 38, No. 1, January–February 2001

Space Station Mir Aerodynamics Along the Descent Trajectory

G. N. Markelov,* A. V. Kashkovsky,† and M. S. Ivanov‡
Institute of Theoretical and Applied Mechanics, 630090, Novosibirsk, Russia

A controlled descent of space station Mir requires the choice of an optimal configuration (positions of solar arrays) that allows one to minimize the disturbing aerodynamic torques and maximize the drag. An approximate approach for choosing the positions based on free-molecular analysis is developed. The aerodynamic characteristics of the chosen configurations are studied by engineering and statistical methods along the descent trajectory. The study showed that a decrease in the flight altitude from 200 to 130 km does not exert a noticeable effect on the magnitude of the force and moment coefficients and also revealed the reasons for the decreasing accuracy of the engineering prediction. It was shown that the gas/surface interaction model significantly affects the torques and, therefore, the choice of the optimal configuration.

Nomenclature

C_A = axial force normalized by $\frac{1}{2}\rho_\infty V_\infty^2 S$
C_m = pitching moment normalized by $\frac{1}{2}\rho_\infty V_\infty^2 SL$
C_n = yawing moment normalized by $\frac{1}{2}\rho_\infty V_\infty^2 SL$
H = altitude, km
Kn = Knudsen number, $\lambda_\infty / L_{\mathrm{LB}}$
L = reference length, 13.6 m
L_{LB} = reference length determining rarefaction effect for local bridging method, m
M_∞ = freestream Mach number
$\bar{M}$ = molecular weight of mixture
S = reference area, 13.5 m^2
T_W = wall temperature, K
T_∞ = freestream temperature, K
V_∞ = freestream velocity, m/s
α = angle of attack, deg
β = sideslip angle, deg
λ_∞ = freestream mean free path, m
ρ_∞ = freestream density, kg/m^3
ϕ = angle of solar array position, deg

Introduction

SPACE objects operating on low Earth orbit have a certain lifetime and will be deorbited after completion of their missions. The plane of their orbits passes both above the world ocean and above the land, including densely populated areas. In the case of uncontrolled descent, these objects usually burn up during reentry, but very heavy or compact ones or parts of them may survive and reach ground, which was the case for several reentering space stations such as Skylab or Salyut-7. They fortunately fell on thinly populated regions.

To reduce possible adverse consequences of collision with the Earth's surface of unburned fragments, which are often rather heavy and fall with a high velocity, controlled descent to the ocean or deserted lands is performed. For space objects with at least limited controllability such as satellites with reaction control system (RCS) thrusters, a controlled choice of proper entry conditions is possible. The object enters the dense layers of the atmosphere with a certain attitude, for which the aerodynamic forces and torques are determined; then, the regions of descent can be predicted rather accurately.

Received 3 March 2000; revision received 23 June 2000; accepted for publication 28 June 2000.

*Senior Research Scientist, Computational Aerodynamics Laboratory; markelov@itam.nsc.ru.
†Research Scientist, Computational Aerodynamics Laboratory.
‡Head, Computational Aerodynamics Laboratory. Senior Member AIAA.

For a controlled descent of a space object, based on available fuel reserve, it is necessary to solve an optimization problem for choosing the object orientation. The combination of aerodynamic forces and disturbing torques for this orientation should allow a possibility of maintaining a definite orientation as long as possible during aerodynamic deceleration of the object after the braking impulse. For the planned descent of the Mir space station (SS), the solution of this problem is significantly complicated because of the very complex shape. It was designed for operation on orbit, and no one ever thought about the problems associated with its deorbiting.

Because of the increase in density along the descent trajectory of the SS Mir, the mechanical and thermal loads significantly increase, and disintegration of the SS Mir begins at a certain altitude. The questions of the proper definition of the SS disintegration and destruction altitudes are beyond the scope of this paper. Based on the accumulated experience on descent of various space objects, in particular, Salyut-7, the beginning of the SS Mir disintegration process into separate parts is expected at an altitude of about 120–130 km. After that, these elements follow different trajectories depending of their size and weight. During the descent of the SS Mir as a single object to the altitude of disintegration, it is possible to use RCS thrusters to maintain the optimum orientation of the SS. This allows a significant reduction of the landing footprints of the fragments over the Earth's surface. Therefore, precise knowledge of the aerodynamic forces and torques of the SS Mir from the orbit to the disintegration altitude is indispensable.

In the range of SS flight altitudes under consideration, freestream conditions vary from free molecular at altitudes above about 200 km to the transitional regime at lower altitudes. Determination of the aerodynamic characteristics of the SS Mir, which has an extremely complex shape, is a complicated problem even if we take into account modern numerical tools for high-altitude aerodynamics.[1–5] Moreover, the SS Mir descent problem is complicated by the necessity of determining the solar array positions that would allow one to minimize the disturbing aerodynamic torques and maximize the drag. The solution of this problem involves multiparametric calculations of aerodynamics for various configurations of the SS Mir, determined by positions of the solar arrays, both in the free-molecular and transitional regimes of rarefied gas flows. The RAMSES[6] software system, which allows one to solve effectively the posed problem of choosing a suitable configuration, was used in the present work. An important aspect here is the question about the accuracy of the local bridging method, which was developed for predicting the aerodynamics of rather simple-shaped bodies. The answer to this question can be obtained only by comparison of the local bridging results with the exact value of aerodynamic characteristics of various modules and solar arrays of the SS Mir in the transitional regime obtained by the direct simulation Monte Carlo (DSMC) method.[7]

The main objective of the present work is a detailed analysis of aerodynamic characteristics of the SS Mir in the free-molecular and transitional regimes and the choice of its optimal configuration for

aeroassisted descent. Particular attention was paid to investigation of applicability of the engineering approach for prediction of high-altitude aerodynamics of the SS Mir by comparison with results of statistical simulation.

Geometric Model

A geometric model of the SS Mir was created using a special subsystem of RAMSES, which ensures the construction of the object geometry from simple geometric elements (primitives) like rectangles, circles, cones, spheres, etc. As an intermediate step, primitives are grouped together to build a compound. These compounds are combined to build compounds of higher levels until the complete model of the space object is constructed. In addition, a panelized surface description of each primitive is provided for numerical analysis.

Figure 1 shows the geometric model of the SS Mir used in this work. Certainly, this model is greatly simplified as compared to the real SS, but it retains all of the basic elements important for aerodynamic studies. The model consists of about 200 primitives and is panelized into about 70,000 triangles. The positions of solar arrays is determined by the angle ϕ. For $\phi = 0$, the solar arrays (except for broken ones) are mounted parallel to the freestream velocity vector at zero angle of attack (Fig. 1). Stationary solar arrays are also marked in Fig. 1. All of the remaining solar arrays [a total of nine pieces on the base block (BB), Kvant, Kvant-2, and Spektr modules] can be rotated with a step of 22.5 deg.

The numerical studies were conducted within the altitude range from 200 to 110 km. The parameters of the atmosphere are borrowed from Ref. 8 and listed in Table 1. The wall temperature was constant for all parts of the SS Mir and equal to $T_W = 350$ K. Diffuse reflection with complete energy accommodation was used as a gas/surface interaction model. The test gas was nonreactive air because the influence of chemical processes in the gas on aerodynamics of the SS Mir are negligible for flight altitudes considered (see details in Ref. 9).

Table 1 Freestream conditions

			Mole fraction				
H, km	ρ_∞, kg/m^3	T_∞, K	X_{O_2}	X_{N_2}	X_O	$\bar{M}$, g/mol	λ_∞, m
110	9.67×10^{-8}	247	0.123	0.770	0.106	27.22	0.599
120	2.27×10^{-8}	368	0.085	0.733	0.183	26.14	2.681
130	8.23×10^{-9}	500	0.071	0.691	0.238	25.43	7.724
140	3.86×10^{-9}	625	0.062	0.652	0.286	24.81	16.920
160	1.32×10^{-9}	822	0.049	0.581	0.370	23.75	50.330
200	3.29×10^{-10}	1026	0.032	0.455	0.514	21.96	196.700

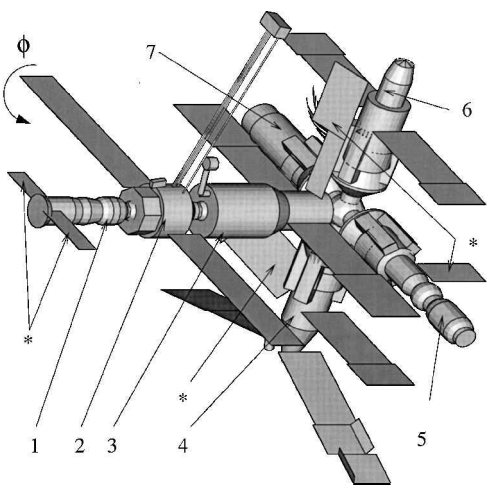

Fig. 1 Module composition of SS Mir: 1, progress spacecraft; 2, Kvant; 3, BB; 4, Spektr; 5, Kristall; 6, Kvant-2; and 7, Priroda; stationary solar arrays are marked by an asterisk.

Results and Discussion

Choice of Configuration

The expected controlled descent of the SS Mir from orbit will be initiated by the braking impulse given by the Progress spacecraft. For a guaranteed shift of the SS Mir to the descent trajectory, because of its mass, it is mandatory to have a rather large reserve of fuel. Therefore, rigorous economy of fuel for maintaining the station attitude is necessary. Hence, the aerodynamic torques created by solar arrays should be reduced, that is, it is necessary to find solar array positions providing the minimum disturbing torques and the maximum drag of the SS Mir. It is also desirable to satisfy an additional condition of static stability of this SS configuration in a narrow range of zero angles of attack and sideslip (from -5 to $+5$ deg). The solution of this problem is complicated by the asymmetry of the SS geometry, the location of the center of mass outside the BB centerline, and the presence of broken solar arrays aligned at significant angles to the flight direction (one on the BB and another on the Spektr).

Obviously, the search for the optimal position of all rotating solar arrays of the SS Mir is a severe problem even for the free-molecular flow regime. Nevertheless, the problem can be slightly simplified by conducting a qualitative analysis of the contribution of some solar arrays to aerodynamic torques. This analysis allows one to assign certain fixed angles of rotation to some solar arrays. For example, the turning of the lower solar arrays of the Spektr module even by a minimum angle (22.5 deg) generates a large pitching moment, which cannot be compensated by rotation of other solar arrays. Therefore, these lower solar arrays of the Spektr module should be aligned in the streamwise direction.

The positions of the remaining seven rotating solar arrays were chosen using a simple approach that allows rejection of SS configurations generating definitely large disturbing torques. This approach consists of three steps.

1) First is sorting of all possible configurations in terms of the magnitude of the disturbing torque. In doing this, the aerodynamic characteristics of different SS configurations were calculated without accounting for mutual shading of the solar arrays and SS modules in the free-molecular regime. In this case, it is possible to determine the total aerodynamic forces and torques of the SS as a sum of the forces and torques produced by each module or solar array at different angles of rotation.

2) Second is refinement of the aerodynamic characteristics of the first 200 configurations accounting for shading and selection of configurations with the greatest values of the drag. (Four configurations considered are shown in Fig. 2 as an example.) Angles of solar array positions for these configurations are listed in Table 2.

3) The third step is the analysis of static stability of these configurations around zero angles of attack and sideslip. This analysis allowed us to choose the most suitable configurations for a subsequent detailed study of their aerodynamics in the transitional regime.

In the two next sections, we consider in detail the aerodynamic characteristics of the SS Mir, which were obtained by engineering and statistical methods in free-molecular and transitional regimes.

Shadow and Multiple Molecule Reflection Effects

When free-molecular flow around concave bodies or space objects with complex shape is considered, it is necessary to take into account the shadowing of one part of the body by other parts (shadow effect) and the incidence of molecules reflected from some parts of the body on other parts (multiple molecule reflections).

To take into account the shadow effect (step 2), the integration code of the RAMSES system was used. The shadowed parts of the

Table 2 Solar array positions for configurations of SS Mir shown in Fig. 2

	Kvant		BB		Kvant-2		
Configuration	Left	Right	Left	Right	Left	Right	Spektr, left
1	90.0	90.0	−22.5	90.0	90.0	90.0	90.0
2	−45.0	−45.0	−45.0	90.0	90.0	67.5	90.0
3	−22.5	−22.5	−22.5	−45.0	−67.5	67.5	−67.5
4	−22.5	−22.5	−22.5	45.0	67.5	67.5	−67.5

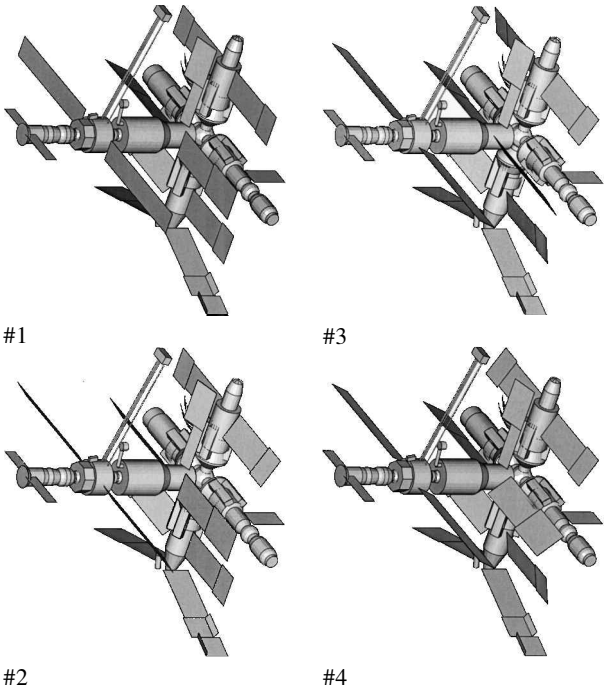

Fig. 2 Geometric configurations of SS Mir.

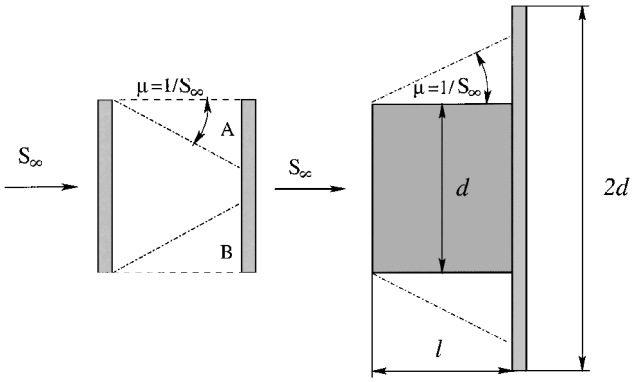

Fig. 3 Semishadow and shielding effects; S_∞ is the freestream speed ratio.

space object are determined by calculating the geometric shadow of all triangular panels in a plane perpendicular to the flow velocity and checking mutual shadowing by comparing the distance to the shadow plane in the case of overlapping shadows. The shadowed parts of the surface are ignored in determining the aerodynamic forces and torques.

The geometric model of the SS Mir consists of 200 primitives and has many concave corner elements; therefore, accounting for only geometric shadowing does not allow one to determine the aerodynamic characteristics with a required accuracy. It is also necessary to take into account the finite Mach number effect (semishadow effect) and multiple reflections. A comparison of the numerical results for aerodynamics of the even more simplified geometric model (50 primitives) of the SS Mir obtained by the integration code and the test particle Monte Carlo (TPMC) method, which ensures complete consideration of the cited effects, shows that the greatest differences are observed in the aerodynamic torques around zero angles of attack and sideslip.[10] Thus, the influence of these effects on the aerodynamics of a more realistic geometric model of the SS Mir was analyzed in detail in the present work.

It is convenient to demonstrate the semishadow effects using simple examples. Figure 3a shows two flat plates located perpendicular to the incoming stream; one of them shadows the other. In this case, the integration code predicts a zero force acting on the aft plate. However, molecules with a significant transverse thermal velocity also hit parts A and B of the aft plate because of the finite Mach number. Thus, accounting for the semishadow effects leads to the emergence of a force load on the shadowed plate.

Nevertheless, the effect of the finite Mach number can also lead to a decrease in the flux of incident particles. For example, in the flow at zero incidence around a body consisting of two coaxial cylinders of different diameters (Fig. 3b), shielding of flux against downstream body parts is observed, that is, the flux of particles onto the end-face part of the backward cylinder decreases. The contribution of the side surface of the first cylinder and the end face of the second cylinder to the total drag of the body is given in Table 3. It is seen that the integration code overestimates the force acting on the body (by 10%) if the dimensionless length of the first cylinder l/d is large enough.

Both semishadow and shielding effects are observed in the flow around the SS Mir. To increase the aerodynamic drag, the solar arrays are aligned at a large angle to the incoming flow, and the effect of semishadow makes the greatest contribution to aerodynamic

Table 3 Influence of dimensionless length l/d on drag normalized by $\frac{1}{2}\rho_\infty V_\infty^2 \pi(d^2/4)$ ($M_\infty = 10$ and $T_\infty/T_W = 3$)

	Total		End face of second cylinder		Side surface of first cylinder	
l/d	TPMC	Integration	TPMC	Integration	TPMC	Integration
0.05	8.93	8.93	6.64	6.68	0.01	0.01
0.25	8.90	8.99	6.58	6.68	0.07	0.07
0.5	8.87	9.05	6.52	6.68	0.13	0.14
1.0	8.83	9.19	6.39	6.68	0.26	0.27
1.5	8.81	9.32	6.24	6.68	0.40	0.40
2.0	8.80	9.46	6.10	6.68	0.52	0.54
3.0	8.81	9.73	5.84	6.68	0.80	0.81
3.5	8.83	9.86	5.74	6.68	0.93	0.94
4.0	8.88	9.99	5.64	6.68	1.07	1.08

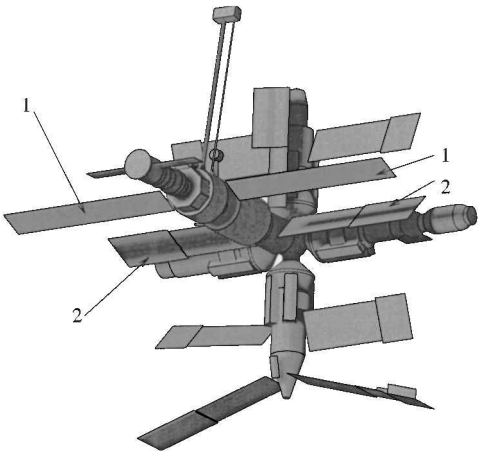

a) Integration method

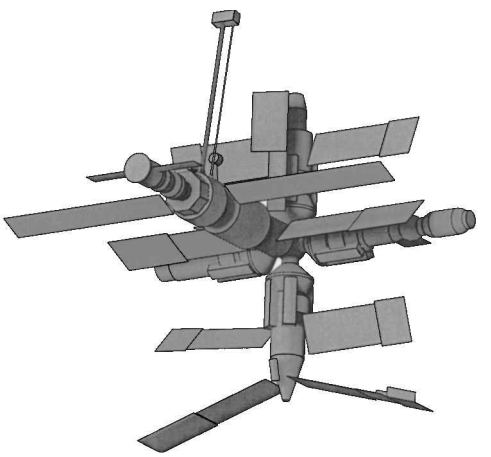

b) TPMC method

Fig. 4 Distribution of axial force coefficient; solar arrays: 1, Kvant, and 2, BB.

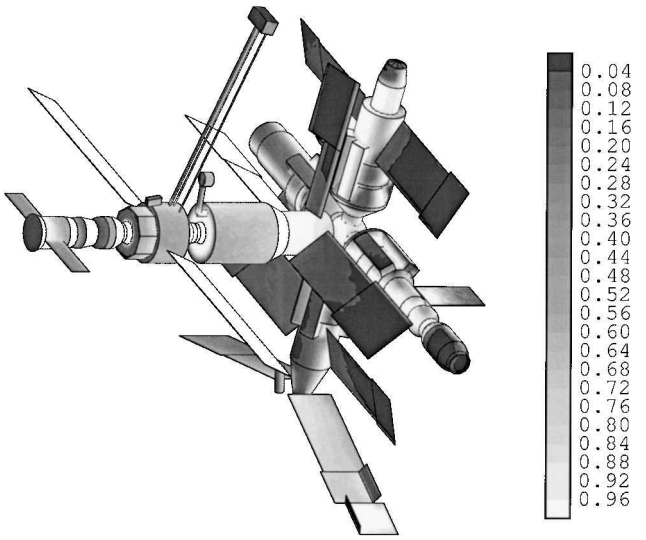

Fig. 5 Contribution of multiple molecule reflections in total particle flux.

characteristics as compared to shielding. Figure 4 shows distributions of the axial force coefficient, which were obtained by the integration and TPMC codes. A significant difference is observed on the BB solar arrays, which are shadowed by the Kvant solar arrays. Taking into account the semishadow effects by the TPMC method increases the axial force $C_A = 50$ in comparison with $C_A = 48$ predicted by the integration code.

The TPMC method also allows the multiple molecule reflections, which cause an additional particle flux on the neighboring body and shadowed parts of the SS Mir, to be taken into account. Figure 5 shows the ratio of the flux of particles arriving on the body surface due to multiple reflections to the total particle flux. This additional particle flux is comparatively small on nonshadowed parts of the surface and rather large on shadowed parts, for example, the backward side of the solar array and BB. The contribution of the multiple reflection effect to the axial force is comparable with the contribution of reflected molecules, but it does not substantially alter the axial force coefficient. The magnitudes of torques produced by the considered configurations in the range of zero angles of attack and sideslip are rather small, and the accuracy of their determination significantly depends on accounting for the finite Mach number effects and multiple reflections.

Careful calculations of the moment characteristics were performed at the last stage of investigation of aerodynamics of the obtained SS configurations in the free-molecular regime to analyze their static stability. Figure 6 shows the behavior of C_n and C_m for four configurations presented in Fig. 2. Note that configuration 1 for which the Kvant solar arrays are aligned perpendicular to the incoming flow to generate the maximum drag (Fig. 7) is statically unstable in terms of the angle of sideslip because these solar arrays are located far upstream of the center of mass. The behavior of the rolling moment is not important in our analysis because rotation around the BB centerline is easily compensated for by RCS thrusters.

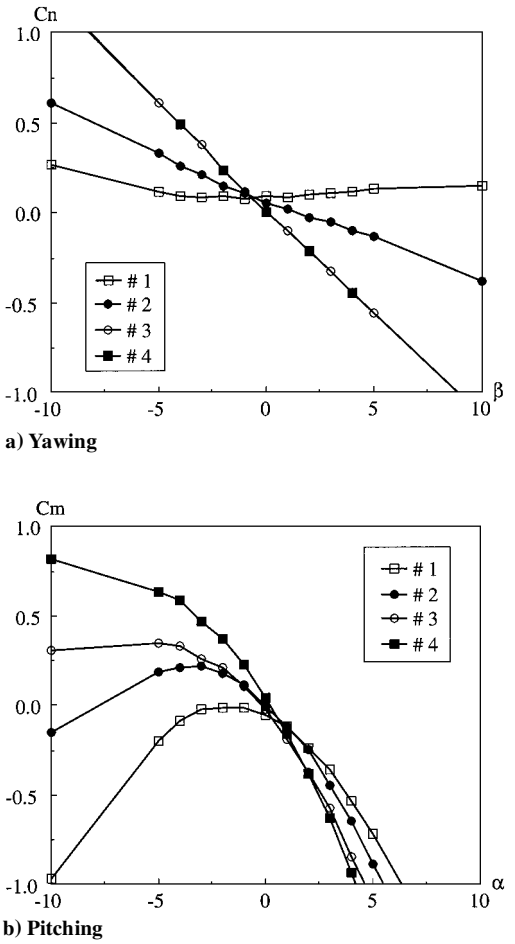

Fig. 6 Moment coefficients vs sideslip angle and angle of attack, respectively, for geometric configurations considered.

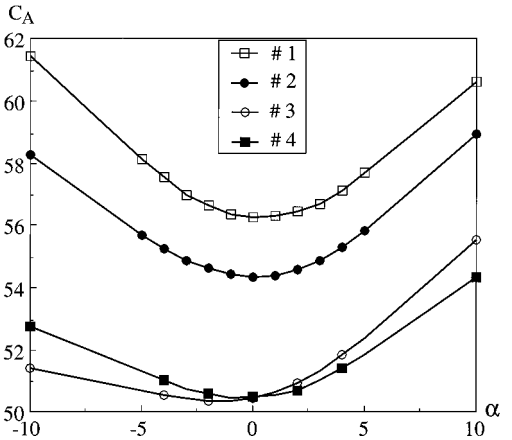

Fig. 7 Axial force coefficients vs angle of attack for geometric configurations considered.

Aerodynamics of SS Mir in Transitional Regime

It is known that the ratio of the contributions of the pressure and friction forces to aerodynamic characteristics changes significantly as the flight altitude decreases, that is, the finite Knudsen numbers are taken into account. This can lead to qualitative differences of SS aerodynamics in the transitional regime as compared to the free-molecular regime. Therefore, the changes in aerodynamic characteristics of the chosen configurations of the SS Mir with changing flight altitude were studied using the local bridging method (LB) implemented in RAMSES, which allows fast multiparametric studies. In this section, the results are presented for aerodynamics of only one configuration (configuration 3 in Fig. 2), which is a compromise between the maximum drag (Fig. 7) and the maximum static stability (Fig. 6). The aerodynamic characteristics of this configuration vs the flight altitude are plotted in Fig. 8, which shows that the force and torque characteristics are almost constant within the altitude range from 200 to 120 km. Significant changes are observed only for the altitudes below 120 km, where the mean free path significantly decreases (Table 1). Thus, the chosen configurations, being optimal in the free-molecular regime, are also suitable for the transitional regime down to the altitude of 120 km.

Figure 8 also shows the axial force and torques obtained in the free-molecular flow around the SS Mir using the TPMC method. Some difference between the LB results for free-molecular limits and the TPMC results is observed. The reason is that LB, as well as the integration code, employs geometrical optics to determine shadowing.

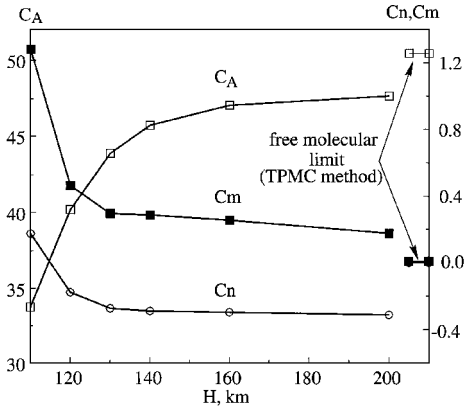

Fig. 8 Aerodynamic characteristics predicted by LB method; $L_{LB} = L$.

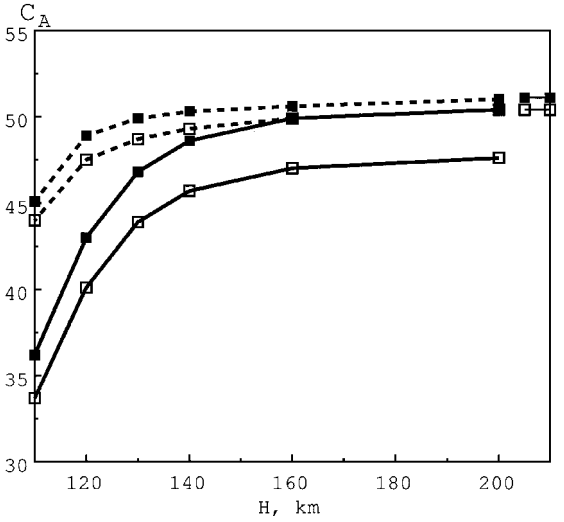

Fig. 9 Axial force coefficient: ——, LB; - - - -, DSMC; □, $\alpha = 0$; and ■, $\alpha = -5$ deg.

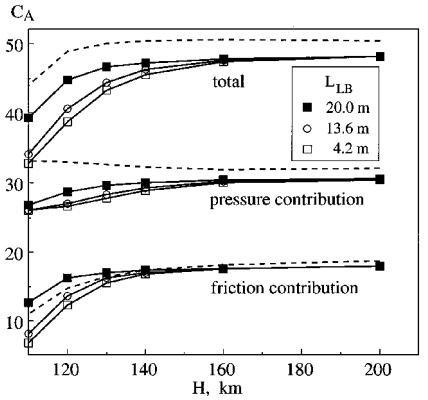

Fig. 10 Influence L_{LB} on LB prediction of axial force coefficient: ——, LB, and - - - -, DSMC, $\alpha = 0$.

The LB approach was constructed using available experimental data for simple bodies, and for such bodies (for example, the Apollo reentry capsule) the LB method produces rather accurate data on aerodynamic characteristics in the transitional regime (for example, see Ref. 3). The prediction accuracy of the LB method for aerodynamics of the SS Mir can be evaluated only by comparing the LB results with the values of forces and torques acting on various elements of the station in the transitional regime obtained by the software system SMILE[11] based on the majorant frequency scheme[12] of the DSMC method.

The C_A values obtained by the LB and DSMC methods are compared in Fig. 9, which shows that LB predicts a lower value of C_A than the DSMC method. Consideration of the contribution of the pressure and friction forces to C_A (Fig. 10) shows that both methods (LB and DSMC) yield almost identical values of the contribution of the friction forces to C_A. At the same time, LB predicts a significantly smaller contribution of the pressure forces than the DSMC method. Possibly, the reason for this difference is again the neglect of the semishadow effects in the LB method.

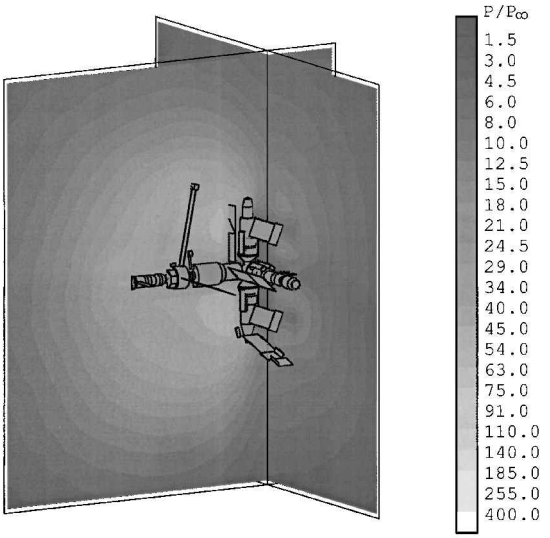

a) $H = 200$ km

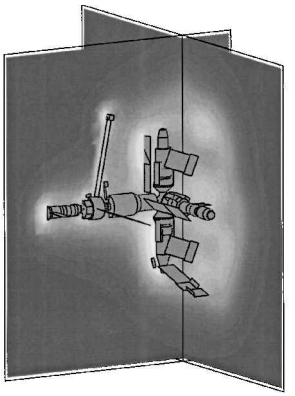

b) $H = 110$ km

Fig. 11 Pressure flowfields.

The change in the flight altitude from 200 to 110 km considerably alters the flow structure around the SS (see Fig. 11, which shows the pressure flowfields obtained by the DSMC method for 200 and 110 km). At a high altitude, the shape of the disturbed region is almost independent of the SS shape and looks like a sphere; at a low altitude, the disturbed region repeats the SS shape. This fact is also illustrated in Fig. 12, which shows the streamlines. Selected streamlines beginning in the vertical plane of symmetry of the BB module change their direction near the basis modules Spektr and Kvant-2. In the near-free-molecular regime (200 km), the pressure is approximately equal near all parts of the SS, whereas the pressure field is substantially nonuniform at the altitude of 110 km, and the maximum values are observed near the Spektr and Kvant-2 modules. This variation of the flowfield leads to the contribution of the pressure forces to the axial force coefficient slightly increasing with decreasing flight altitude (Fig. 10). For aerodynamic shapes, this contribution slightly decreases, which is used in the development of the LB method. This is the reason for the difference in the dependence of the contribution of the pressure forces on the altitude between the LB and DSMC methods, while the contribution of the friction forces is roughly identical.

Note that the use of LB for analysis of aerodynamics in the transitional regime of an extremely complex object such as the SS Mir is rather unusual. This is primarily because the development of LB is based on knowledge about the flow around blunted bodies. The SS Mir consists of both blunted sealed modules and solar arrays of

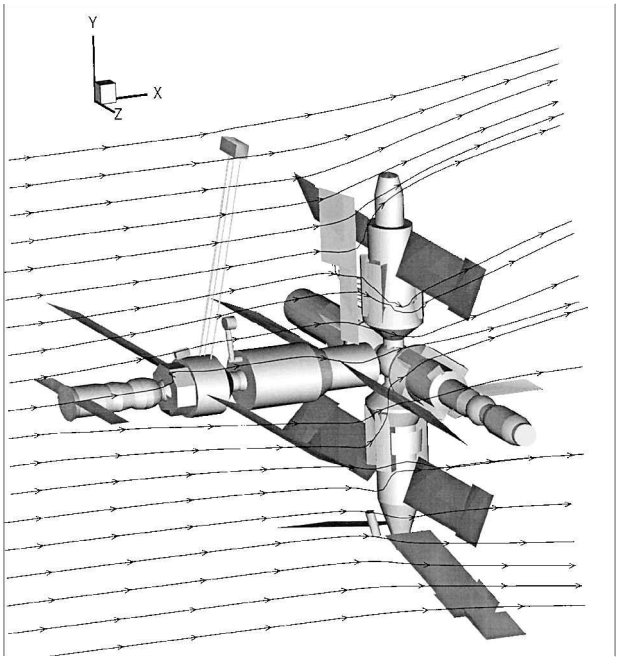

Fig. 12 Selected streamlines: H = 110 km, DSMC.

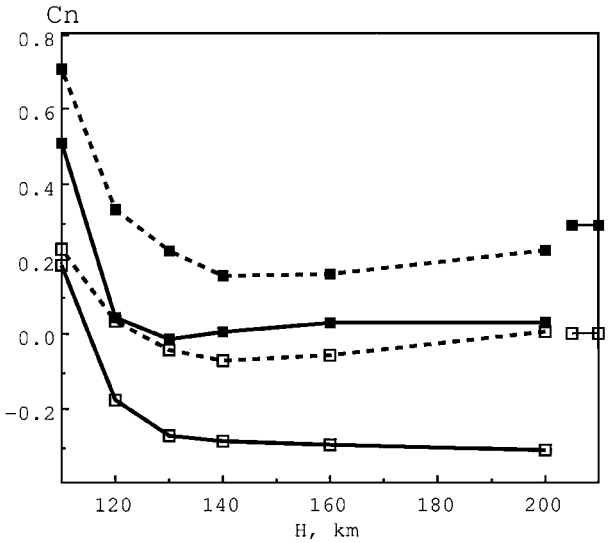

Fig. 13 Yawing moment coefficient: ——, LB; - - - -, DSMC; □, $\alpha = 0$; and ■, $\alpha = -5$ deg.

large area located at low angles of attack. Also, there is some complexity in choosing the reference length L_{LB}, which determines the effect of flow rarefaction ($Kn = \lambda_\infty / L_{\mathrm{LB}}$). For blunted bodies, for example, for a reentry capsule, the reference length L_{LB} used to determine the Knudsen number is the diameter of the body. However, in using LB for determination of the characteristics of the SS Mir, the choice of the proper value of the reference length is not so obvious. Calculations were conducted for three values of L_{LB} to study the effect of the reference length on LB predictions. The minimum value of L was chosen as a certain mean diameter of sealed modules ($L_{\mathrm{LB}} \propto 4$ m). The maximum value of the reference length was determined as $\propto \sqrt{S_p}$, where S_p is the area of the SS projection onto a plane perpendicular to the incoming flow. The third value was the mean arithmetic of the first two. The effect of the reference length on the axial force is shown in Fig. 10: This effect is insignificant above altitudes of 140 km. At the altitude of 120 km, the closest coincidence between the LB and DSMC results for the contribution of the friction forces is observed for the mean arithmetic value of L_{LB}, which was chosen for subsequent studies.

A comparison of the moment coefficients C_n and C_m obtained by the LB and DSMC methods for angles of attack $\alpha = 0$ and 5 deg is shown in Figs. 13 and 14. Qualitative agreement between the

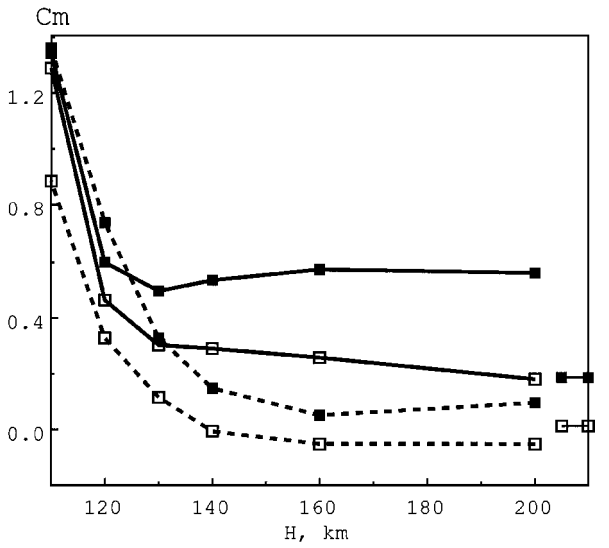

Fig. 14 Pitching moment coefficient: ——, LB; - - - -, DSMC; □, α = 0; and ■, $\alpha = -5$ deg.

LB and DSMC results is observed, but quantitive differences are significant, which suggests the need to improve the LB method for these complex geometries.

Influence of Gas/Surface Interaction Model

The accuracy of the calculation of the aerodynamic characteristics depends significantly on the gas/surface interaction model. The choice of a proper model is particularly important at high altitudes (orbital flight) where the collision of molecules with the body surface plays the dominant role.

The gas/surface interaction models for the DSMC and TPMC methods should provide analytical expressions for reflected velocity distribution functions. There are several applicable models such as the specular-diffuse model, Nocilla[13] model, and Cercignani–Lampis–Lord (CLL) model (see Ref. 14). For moderate to high energy scattering from industrial surfaces, the flux distribution of scattered molecules frequently has a lobular shape. Whereas the diffuse reflection does not allow one to take into account such behavior, the Nocilla[13] and CLL models are developed to handle it.

The known Nocilla velocity distribution function is

$$f = n_r \pi^{-\frac{3}{2}} c_r^{-3} \exp\left\{-c_r^{-2}\,[\boldsymbol{\xi} - c_r \boldsymbol{S}_r]^2\right\}$$

$$c_r = \sqrt{2\,k/m\;T_r}, \qquad \boldsymbol{S}_r = \boldsymbol{\xi}_r / c_r \tag{1}$$

This distribution function contains the four parameters n_r, T_r, $\boldsymbol{S}_r \equiv (S_{nr}$ and $S_{\tau r})$ that characterize the density, temperature, and velocity of this reflected gas. In Ref. 15, the values of these parameters were determined by using the results of laboratory experiments. In these experiments, the force action of molecular beams on samples of engineering materials of satellites' external coating and scattering distribution of molecules reflected from the surface were measured. Numerical values for four parameters of the Nocilla[13] model for a number of typical engineering materials used in aerospace applications were presented in Ref. 15. Therefore, this model was implemented in software systems RAMSES and SMILE for high-altitude aerodynamics simulation.

To estimate the effect of the gas/surface interaction model, the flow around the SS Mir was calculated by the TPMC and DSMC methods with the Nocilla[13] model. To simulate the reflection of molecules from the solar array, we used the Nocilla model parameters fitted for glass, engineering surface of solar arrays, and for screen–vacuum glass cloth, engineering surface of external coating of all other surfaces.

The effect of gas/surface interaction is most clearly demonstrated by the behavior of the pressure C_p and shear stress C_τ coefficients in a free-molecular flow past a flat plate with an angle of attack

Table 4 Influence of reflection model on aerodynamic coefficients

	Free-molecular flow		120 km	
	Diffuse	Nocilla[13]	Diffuse	Nocilla
C_A	50.48	54.39	47.60	48.87
C_n	0.00	0.41	0.04	0.20
C_m	0.01	1.49	0.32	1.11

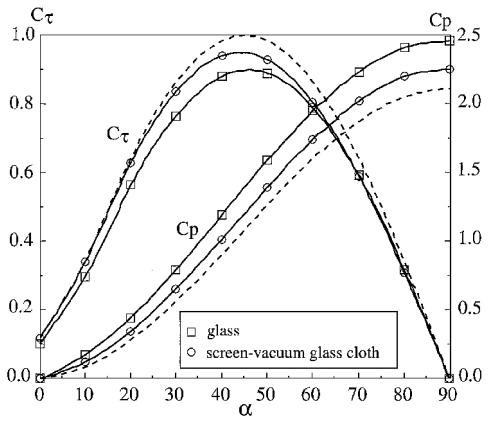

Fig. 15 C_p and C_τ coefficients for different engineering surfaces: ——, Nocilla[13] model, and - - - -, diffuse model, where $M_\infty = 10$ and $T_\infty/T_W = 3$.

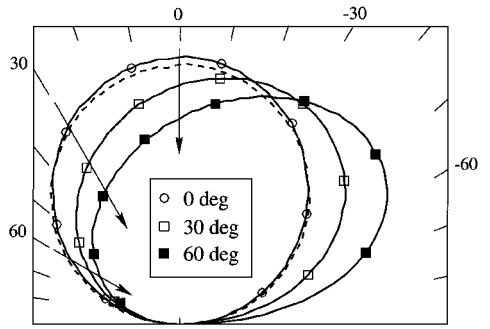

Fig. 16 Influence of incidence angle on angular density distribution: ——, Nocilla[13] model for glass engineering surface, and - - - -, diffuse model, where $M_\infty = 10$ and $T_\infty/T_W = 3$.

(Fig. 15). The use of the Nocilla[13] model with parameters fitted for reflection from glass and screen–vacuum glass cloth surfaces increases the pressure coefficient (up to 15% for $\alpha = 90$ deg) and decreases the shear stress coefficient (up to 10% for $\alpha = 45$ deg) in comparison with diffuse reflection. An angular density distribution strongly depends on the angle of incidence of the particles onto the surface (Fig. 16). Upon normal incidence, scattering is close to diffuse reflection; as the angle of incidence increases, the scattering diagram is inclined toward the angle of specular reflection and elongated.

Table 4 shows a comparison of calculation results for aerodynamics of the SS Mir obtained by the Nocilla[13] and diffuse reflection models for two flight altitudes. In the free-molecular regime, the difference in C_A is less than 10%, though the contribution of reflected molecules to C_A differs by more than a factor of three (6.7 for the Nocilla model and 2.0 for diffuse reflection). This insignificant increase in C_A is explained by the determining contribution being made by incident molecules. The difference in other aerodynamic characteristics determined mainly by reflected molecules can reach one order of magnitude and even more (see C_n and C_m). Naturally, for a lower Knudsen number (120 km), this difference in aerodynamic characteristics is much smaller (see Table 4), and the flowfields become similar.

This unexpected strong effect of the gas/surface interaction model on the torques made us repeat choosing a suitable configuration of the SS Mir using the Nocilla[13] model for gas/surface interaction.

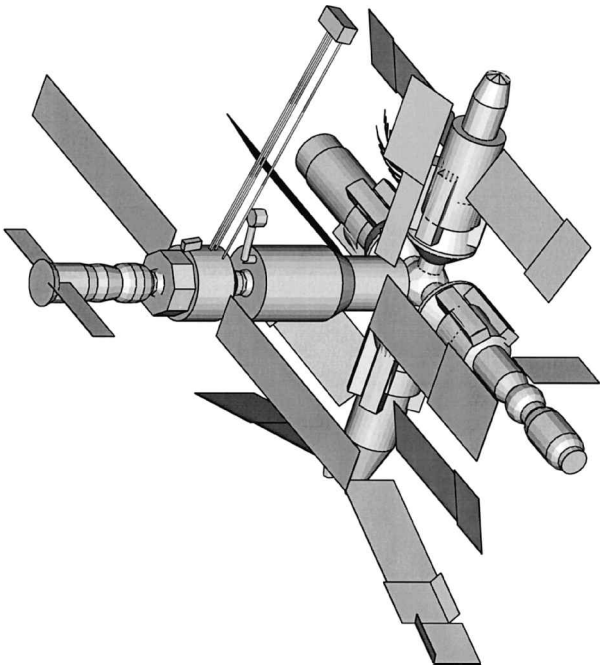

Fig. 17 Configuration of SS Mir chosen with Nocilla[13] model for gas/surface interaction.

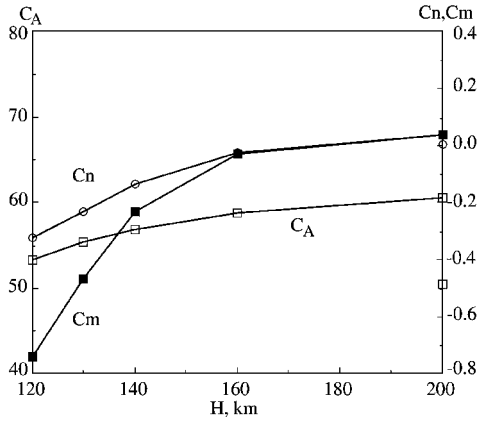

Fig. 18 Axial force and moment coefficients for the chosen configuration with Nocilla[13] model for gas/surface interaction.

First, a configuration with shadowing ignored was chosen in the free-molecular regime using the algorithm mentioned at the beginning of this section. The aerodynamic characteristics were refined, and the static stability was studied (steps 2 and 3) using the TPMC method because it was shown, for the diffuse reflection case, that this method allows one to take into account the semishadow and multiple reflection effects. One of the chosen configurations is shown in Fig. 17. The analysis of aerodynamics of this configuration along the descent trajectory showed that the force and moment coefficients change insignificantly above altitudes of 140 km (Fig. 18). Thus, the chosen SS Mir configuration retains low disturbing torques along the descent trajectory until the disintegration altitude.

Conclusions

The aerodynamic characteristics of the SS Mir in the free-molecular regime have been studied in detail using engineering and statistical methods. Reasons (semishadow and multiple reflection effects) for decreased accuracy of the engineering prediction of aerodynamic characteristics of an extremely complex space object such as the SS Mir have been revealed.

An approximate approach for choosing configurations of the SS Mir (positions of the solar arrays) with required characteristics for its controlled descent from the orbit has been developed. This approach consists of three sequential steps at which unsuitable configurations of the SS Mir in free-molecular regime are rejected.

Investigations of the aerodynamic characteristics of the chosen configurations in the transitional regime (flight altitudes of 200–110 km) conducted by the DSMC method show that a decrease in the flight altitude from 200 to 130 km does not exert a noticeable effect on the magnitude of the force and moment coefficients nor on the static stability. It is shown that the use of the Nocilla[13] model leads to some increase in the axial force of the SS Mir and to significant changes in the torques as compared with their values at diffuse reflection.

Note that only the combined use of the entire modern arsenal of numerical methods of high-altitude aerothermodynamics allowed us to study the aerodynamic portion of the overall problem of the planned controlled descent of the SS Mir. The DSMC and engineering methods are by no means opposed to each other, and it is beneficial to use them together.

Acknowledgments

The authors would like to express their thanks to L. V. Mishina and A. N. Krylov from Rocket Space Corp. "Energia" for initializing this study and for fruitful discussions.

References

[1]Rault, D. F. G., "Aerodynamics of Shuttle Orbiter at High Altitudes," *Journal of Spacecraft and Rockets*, Vol. 31, No. 6, 1994, pp. 944–952.

[2]Wilmoth, R. G., LeBeau, G. J., and Carlson, A. B., "DSMC Grid Methodologies for Computing Low-Density, Hypersonic Flows About Reusable Launch Vehicles," AIAA Paper 96-1812, June 1996.

[3]Ivanov, M. S., Markelov, G. N., Gimelshein, S. F., Mishina, L. V., Krylov, A. N., and Grechko, N. V., "High-Altitude Capsule Aerodynamics with Real Gas Effects," *Journal of Spacecraft and Rockets*, Vol. 35, No. 1, 1998, pp. 16–22.

[4]Moss, J. N., Blanchard, R. C., Wilmoth, R. G., and Braun, R. D., "Mars Pathfinder Rarefied Aerodynamics: Computations and Measurements," AIAA Paper 98-0298, Jan. 1998.

[5]Wilmoth, R. G., Rault, D. F. G., Shane, R. W., and Tolson, R. H., "Rarefied Aerothermodynamics Predictions for Mars Global Surveyor," *Proceedings of the XXI International Symposium on Rarefied Gas Dynamics*, edited by R. Brun, R. Campargue, R. Gatignol, J.-C. Lengrand, Vol. 2, Cepadues Editions, Toulouse, France, 1999, pp. 673–680.

[6]Koppenwallner, G., Johannsmeier, D., Klinkrad, H., Ivanov, M., and Kashkovsky, A., "A Rarefied Aerodynamic Modelling System for Earth Satellites (RAMSES)," *Proceedings of the XIX International Symposium on Rarefied Gas Dynamics*, edited by J. Harvey and G. Lord, Vol. 2, Oxford Univ. Press, Oxford, 1995, pp. 1366–1372.

[7]Bird, G., *Molecular Gas Dynamics and the Direct Simulation of Gas Flows*, Clarendon, Oxford, 1994, Chap. 9.

[8]Dogra, V. K., Wilmoth, R. G., and Moss, J. N., "Aerothermodynamics of 1.6-m-Diameter Sphere in Hypersonic Rarefied Flow," AIAA Paper 91-0773, Jan. 1991.

[9]Markelov, G. N., Kashkovsky, A. V., and Ivanov, M. S., "Space Station "Mir" Aerodynamics Along the Descent Trajectory," AIAA Paper 2000-0637, Jan. 2000.

[10]Ivanov, M. S., Markelov, G. N., Kashkovsky, A. V., and Gimelshein, S. F., "Statistical Simulation of High-Altitude Aerodynamics Problems," *Proceedings of the III European Symposium on Aerothermodynamics for Space Vehicles*, SP-426, ESA, 1998, pp. 245–252.

[11]Ivanov, M. S., Markelov, G. N., and Gimelshein, S. F., "Statistical Simulation of Reactive Rarefied Flows: Numerical Approach and Applications," AIAA Paper 98-2669, June 1998.

[12]Ivanov, M. S., and Rogasinsky, S. V., "Theoretical Analysis of Traditional and Modern Schemes of the DSMC Method," *Proceedings of the XVII International Symposium on Rarefied Gas Dynamics*, edited by A. Beylich, VCH, Aachen, Germany, 1991, pp. 629–642.

[13]Nocilla, S., "The Surface Re-Emission Law in Free Molecule Flow," *Proceedings of the III International Symposium on Rarefied Gas Dynamics*, Vol. 1, Academic Press, New York, 1963, pp. 327–346.

[14]Lord, R. G., "Some Further Extensions of the Cercignani–Lampis Gas–Surface Interaction Model," *Physics of Fluids* Vol. 7, No. 5, 1995, pp. 1159–1161.

[15]Musanov, S. V., Nikiforov, A. P., Omelik, A. L., and Freedlender, O. G., "Experimental Determination of Momentum Transfer Coefficients in Hypersonic Free Molecular Flow and Distribution Function Recovery of Reflected Molecules," *Proceedings of the XIII International Symposium Rarefied Gas Dynamics*, edited by O. Belocerkovsii, M. Kogan, S. Kutateladze, and A. Rebrov, Vol. 1, Plenum, New York, 1985, pp. 669–676.

J. C. Taylor
Associate Editor